frontiers in Physiology

ORIGINAL RESEARCH
published: 08 June 2021
doi: 10.3389/fphys.2021.654928

Localized Oxygen Exchange Platform for Intravital Video Microscopy Investigations of Microvascular Oxygen Regulation

Richard J. Sové[1], Stephanie Milkovich[2], Hristo N. Nikolov[3], David W. Holdsworth[2,3], Christopher G. Ellis[2†] and Graham M. Fraser[4†]*

[1] Department of Biomedical Engineering, Johns Hopkins University School of Medicine, Baltimore, MD, United States, [2] Department of Medical Biophysics, University of Western Ontario, London, ON, Canada, [3] Robarts Research Institute, University of Western Ontario, London, ON, Canada, [4] Division of BioMedical Sciences, Faculty of Medicine, Memorial University of Newfoundland, St. John's, NL, Canada

OPEN ACCESS

Edited by:
Antonio Colantuoni,
University of Naples Federico II, Italy

Reviewed by:
Ivo P. Torres Filho,
United States Army Institute of Surgical Research, United States
Dominga Lapi,
University of Naples Federico II, Italy
Romeo Martini,
University Hospital of Padua, Italy

***Correspondence:**
Graham M. Fraser
graham.fraser@med.mun.ca

[†]These authors have contributed equally to this work and share senior authorship

Specialty section:
This article was submitted to Vascular Physiology, a section of the journal Frontiers in Physiology

Received: 17 January 2021
Accepted: 23 March 2021
Published: 08 June 2021

Citation:
Sové RJ, Milkovich S, Nikolov HN, Holdsworth DW, Ellis CG and Fraser GM (2021) Localized Oxygen Exchange Platform for Intravital Video Microscopy Investigations of Microvascular Oxygen Regulation. Front. Physiol. 12:654928. doi: 10.3389/fphys.2021.654928

Intravital microscopy has proven to be a powerful tool for studying microvascular physiology. In this study, we propose a gas exchange system compatible with intravital microscopy that can be used to impose gas perturbations to small localized regions in skeletal muscles or other tissues that can be imaged using conventional inverted microscopes. We demonstrated the effectiveness of this system by locally manipulating oxygen concentrations in rat *extensor digitorum longus* muscle and measuring the resulting vascular responses. A computational model of oxygen transport was used to partially validate the localization of oxygen changes in the tissue, and oxygen saturation of red blood cells flowing through capillaries were measured as a surrogate for local tissue oxygenation. Overall, we have demonstrated that this approach can be used to study dynamic and spatial responses to local oxygen challenges to the microenvironment of skeletal muscle.

Keywords: microcirculation, blood flow, oxygen transport, microfluidics, capillary, oxygen saturation, mathematical modeling

1. INTRODUCTION

Oxygen (O_2) regulation is a critical physiological function where precise regulatory control is required to ensure the metabolic demands of the tissues of the body are met (Duling, 1972; Sparks, 1980; Kontos and Wei, 1985; Golub and Pittman, 2013). In order for such a level of control to be possible, there must be various mechanisms in place to sense O_2 demand and correspondingly adjust O_2 supply. Numerous studies have confirmed that the presence or absence of O_2 in the microcirculation results in a vasoactive response such that high levels of O_2 result in vasoconstriction (Duling, 1972; Hutchins et al., 1974; Welsh et al., 1998; Zhu et al., 1998; Frisbee and Lombard, 2002) and low levels of O_2 result in vasodilation (Pittman and Duling, 1973; Fredricks et al., 1994; Frisbee et al., 2002). These findings allude to the existence of an O_2 sensor, the location of which remains unclear (Jackson, 2016). Potential locations include the red blood cell (RBC), arteriolar smooth muscle, arteriolar endothelium and even extra-vascular cells; see Jackson (2016) for an in-depth review.

There has been substantial evidence pointing to the RBC as the sensor for O_2 in the microcirculation; see review by Ellsworth et al. (2009). One potential mechanism that has been

proposed is the O_2-dependent release of ATP from RBCs. In this mechanism, ATP is released from RBCs in response to decreased oxyhemoglobin saturation leading to increased plasma ATP (Bergfeld and Forrester, 1992; Ellsworth et al., 1995). The intra-luminal ATP can then bind to P_{2Y2} receptors on the blood vessel endothelium triggering an upstream vasodilatory response (Sprague et al., 1996; McCullough et al., 1997; Collins et al., 1998; Dietrich et al., 2000). Several pathological conditions have been associated with an impaired ability to release ATP, such as sepsis (Bateman et al., 2015) and type II diabetes (Sprague et al., 2006; Hanson et al., 2009; Ellis et al., 2010), potentially affecting the ability to regulate oxygen.

Various studies have used microscopy in conjunction with methods to alter the tissue oxygenation to interrogate the regulatory system (Welsh et al., 1998; Frisbee and Lombard, 2002; Frisbee et al., 2002). For instance, suffusion solutions with varying levels of O_2 have been used to control O_2 in several tissue preparations to study the regulatory response (Frisbee and Lombard, 2002; Frisbee et al., 2002). In previous studies, we used intravital video microscopy that combines a gas exchange platform with computer controlled gas flow meters to manipulate the gas composition at the surface of rat *extensor digitorum longus* (EDL) muscle to study the response of the microcirculation to a range of O_2 concentrations (Jagger et al., 2004; Ellis et al., 2006; Milkovich et al., 2007). In these studies, the entire surface of the muscle was affected by the change in O_2. While these approaches were able to elicit vasodilatory responses, more localized changes in O_2 could potentially reveal information leading to the location of the O_2 sensor.

More recently, a localized micro-delivery system was developed that was capable of limiting the change in RBC oxygen saturation (SO_2) to a circular area of approximately 175 μm in diameter (Ghonaim et al., 2011), however, changes in RBC supply rate (SR) were not reported (Ghonaim et al., 2011). This finding was supported by a mathematical model of the regulatory system that suggests the signal for vasodilation is additive and depends on the number of capillaries that are stimulated (Ghonaim et al., 2013). A later study used a larger exchange window (1 mm long by 0.1 mm wide) to manipulate the RBC SO_2 of a much larger area; this larger exchange window elicited a flow response (Ghonaim, 2013). This work further supports the idea that the vasodilatory signal is additive.

The work in Ghonaim (2013) showed promising results which were consistent with the proposed ATP release mechanism, however, there were some limitations for studying O_2 regulatory mechanisms. First, stimulating multiple microvascular units at the same time potentially affects multiple feeding arterioles. Additionally, the setup in Ghonaim et al. could only resolve capillaries that were less than 60 μm from the surface; one challenge associated with using gas exchange chambers with intravital microscopy is that the chamber must be placed in between the objective and the muscle, reducing the focal depth to which the vasculature can be resolved. This impedes the ability to focus on structures deeper in the tissue.

The objective of the present study was to develop and validate a modular gas exchange device capable of changing local tissue O_2 tension in micro-scale volumes and thus manipulating oxygen saturations within the overlying capillaries. One potential benefit of such a device is to determine if stimulation of a small number of microvascular units is sufficient to elicit a flow response. By making the design modular, the device can be easily adjusted to suit different needs and available equipment. For example, the shape and size of the exchange surfaces can easily be changed. This design also aims to maximize the resolvable depth permitted by the microscope objective's working distance in order to visualize structures deeper in the tissue as well as allowing for recording of adjacent regions in the tissue. In addition, we used a graphical processing unit (GPU) accelerated computational model of oxygen transport to estimate O_2 content in the tissue and the temporal affects of changing O_2 in the chamber. Overall, we describe a novel modular gas exchange device for studying microvascular oxygen regulation *in vivo* in tissues that can be imaged using conventional inverted microscopes.

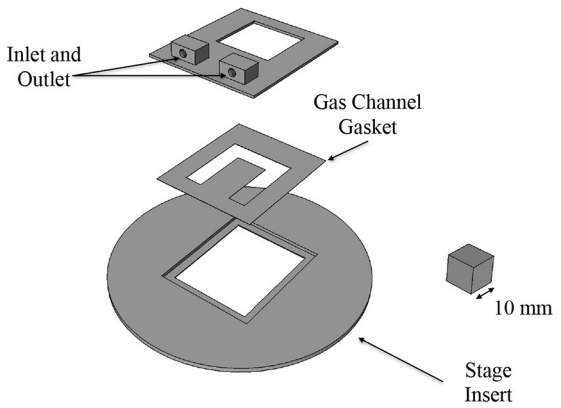

FIGURE 1 | Three dimensional CAD model of gas chamber components. Inlet/outlet mount and stage insert were 3D printed. The gas channel gasket was made out of polymethyl-methacrylate (PMMA). The gas channel is sealed on the bottom with a glass coverslip and on the top with a glass coverslip patterned with laser-cut exchange windows.

2. METHODS

2.1. Gas Exchange Chamber Design and Fabrication

The gas exchange chamber was comprised of a microscope stage insert, a gasket to form the side walls of the gas channel and a platform for the inlet and outlet of the channel (see **Figure 1**). The bottom of the channel was closed by a replaceable glass coverslip. The top of the channel was sealed by a custom, laser-cut 24 x 30 mm glass coverslip with five windows for gas exchange using a process described in Nikumb et al. (2005); the windows were mated with a thin, gas-permeable, membrane. The components were assembled together using vacuum grease to prevent gas leakage.

The stage insert and platform for the inlet and outlet were designed in FreeCAD and 3D printed. The gasket was fabricated by hand cutting 100 μm thick sheets of polymethyl-methacrylate

(PMMA) to the desired shape. The gas-permeable membrane was fabricated in polydimethylsiloxane (PDMS) using a spin-coating technique similar to McDonald et al. (2000). PDMS (Sylgard 184, Dow Corning Corporation) in a 10:1 prepolymer to cross-linker ratio by weight was spin-coated at 1,700 rpm for 30 s; resulting membranes were approximately 25 μm in thickness.

Gas composition (O_2, CO_2, and N_2) was controlled using computer controlled mass flow meters that imposed square wave oxygen oscillations within the exchange chamber consisting of 1 min of 5% O_2 followed by 2 min of 12%, 2 min of 2%, and 1 min of 5% with static 5% CO_2 and balance N_2. Gas temperature was maintained at 37°C.

2.2. Animal Preparation

Four male Sprague-Dawley rats were allowed to acclimatize in animal facilities for 8–11 days prior to testing. Animals were group housed in a climate controlled room maintained between 21 and 24°C, with humidity of 25–40%, and a 12 h light/dark cycle. Animals were provided water and rat chow *ad libitum*. Animal weights ranged between 150 and 200 g on the day of testing. Rats were anesthetized with sodium pentobarbital (65 mg/kg) via intraperitonial injection. Prior to instrumentation, surgical plane of anesthesia was determined by the absence of palpebral, and toe pinch withrdrawal reflexes. Depth of anesthesia was repeatedly assessed over the duration of animal testing. Once surgical plane was achieved animals were instrumented with arterial and venous indwelling catheters and tracheotomized for ventilation as previously described (Ellis et al., 1992, 2010). Animals were mechanically ventilated with 30% oxygen and balance nitrogen while their inspired O_2, heart rate, and blood pressure levels were continuously monitored to verify a normotensive state during data collection (mean arterial pressure > 70 mmHg) as described in Ellis et al. (2010). The *extensor digitorum longus* (EDL) muscle of the hind limb was prepared for microscopy as described in Fraser et al. (2012); this preparation was based on that by Tyml and Budreau (1991). The muscle was reflected on the 3D printed gas exchange chamber fitted into the microscope stage (**Figure 2**), and secured using suture attached to the distal tendon of the muscle. The muscle was then covered with oxygen-impermeable polyvinylidene film (Saran Wrap, Dow Corning) and a glass coverslip to isolate it from the room air. The tissue was trans-illuminated with a 75 W xenon lamp (Olympus U-LH75XEAPO) using an Olympus IX-81 inverted microscope equipped with 10X (Olympus U Plan S-APO; 0.4 NA) and 20X (Olympus U Plan LWD; 0.45 NA) objectives. The corresponding images were captured using the dual video camera system similar to that previously described in Arpino et al. (2017). During data collection, animal core temperatures were continuously monitored using a rectal thermocouple and maintained between 36 and 37 C using a heat lamp. Following data collection animals were euthanized with an injection of sodium pentobarbital (150 mg/kg) into the carotid artery cannula. The experiments used in this study were approved by the University of Western Ontario's Animal Care and Use Committee.

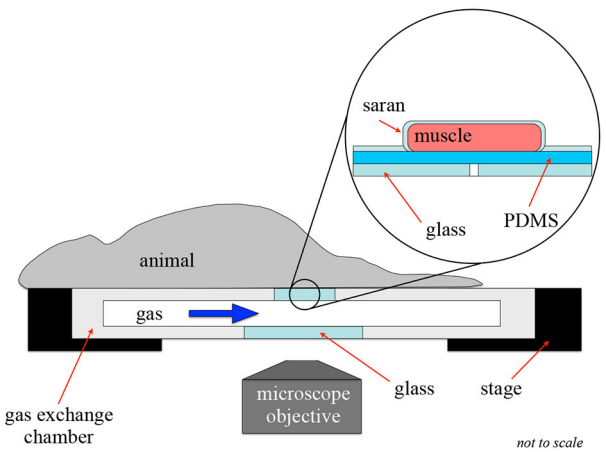

FIGURE 2 | Intravital video microscopy experimental setup. This figure shows the experimental setup for an intravital experiment to allow for oxygen exchange to a localized area of tissue. In this setup, the muscle is extended over the gas exchange window and covered in gas-impermeable Saran wrap to isolate the muscle from the surrounding environment.

TABLE 1 | Parameters used in mathematical model.

Parameter	Value	References
D	2.41×10^{-5} cm^2/s	Bentley et al., 1993
k	3.89×10^{-5} mL O_2/mL/mmHg	Mahler et al., 1985
D'	3.40×10^{-5} cm^2/s	Merkel et al., 2000
k'	1.32×10^{-5} mL O_2/mL/mmHg	Shiku et al., 2006
M_0	1.57×10^{-4} mL O_2/mL/s	Sullivan and Pittman, 1984
K	30 mmHg/s	Goldman, 2008
P_0	48 mmHg	Goldman, 2008
P_{50}	0.5 mmHg	Honig and Gayeski, 1982

2.3. Data Analysis and Statistics

Intravital video microscopy images were acquired at 21 frames per second at two wavelengths, 438 and 450 nm using a beam splitter (Dual Cam 2, Photometrics) and two Rolera XR digital video cameras. Video sequences were processed to generate functional images (e.g., minimum intensity image) that define the location of flowing blood vessels due to the passage of red blood cells which strongly absorb light at the wavelengths selected (Japee et al., 2004). Images were analyzed offline using software developed in MATLAB (Mathworks) to quantify SO_2 and hemodynamics via selection of individual capillaries in a semi automated fashion from functional images as described previously (Japee et al., 2004, 2005a,b; Fraser et al., 2012). SO_2 and SR values for individual capillaries were binned every 5 s and presented as the mean of the bin to show representative responses in single vessels. Capillary RBC SO_2, RBC SR, velocity, and hematocrit responses for all sampled capillaries were grouped based on proximity to the exchange window in the x-y plane (directly overlying the window, <100 μm from the window, 100–200 μm from the window, and >200 μm from the window) and statistical

comparisons were made for each imposed gas exchange chamber oxygen concentration ($[O_2]$). Capillary data sets were tested for deviation from normal distributions using Shapiro-Wilk tests, and Brown-Forsythe tests were used to evaluate differences in group variances. All normally distributed capillary data was paired across oxygen perturbations and repeated measures one-way analysis of variance (ANOVA) with Tukey's multiple comparison test was used to identify significant differences. Similarly, non-normally distributed capillary data was grouped by oxygen perturbations and Friedman tests with Dunn's multiple comparison post test was used to identify significant differences. A p value of < 0.05 was considered significant across all comparisons. All tests were performed using Prism 9 (Graphpad). Means and standard deviations are reported unless otherwise noted.

2.4. Mathematical Model of Tissue Oxygenation

A mathematical model of tissue oxygenation is used to determine the extent of oxygen diffusion in the tissue from the gas exchange chamber. Oxygen diffusion through tissue and the thin (∼25 μm) PDMS barrier between tissue and the glass slide was modeled in 3D over time. Tissue oxygen partial pressure (PO_2) was determined by numerically solving:

$$k\frac{\partial P}{\partial t} = Dk\nabla^2 P + Kk\left(1 - \frac{P}{P_0}\right) - M_0\frac{P}{P + P_{50}}, \in \Omega_{\text{tissue}},$$

$$k'\frac{\partial P}{\partial t} = D'k'\nabla^2 P, \in \Omega_{\text{PDMS}},$$

where D/D' and k/k' are oxygen diffusivity and solubility in tissue/PDMS, respectively, M_0 is the maximal tissue oxygen consumption, P_{50} is the PO_2 at which consumption is half M_0, P_0 is the average capillary PO_2 and K is the rate of oxygen transport from the capillaries into the tissue. Ω_{tissue} and Ω_{PDMS} represent the tissue and PDMS domains, respectively. The parameters used in our model are summarized in **Table 1**.

This model assumes the tissue is homogeneously consuming oxygen and that there is a homogeneous supply of oxygen from the capillaries. Zero flux boundary conditions were specified for the tissue boundaries and along the glass surface. Fixed PO_2 boundary conditions matching those employed in *in vivo* experiments were applied at the surface of the gas exchange window. Similar models were implemented in previous studies to predict tissue oxygenation (Goldman, 2008; Ghonaim et al., 2011). Our model also includes transport through the PDMS layer directly above the gas exchange window which was not incorporated in previous models.

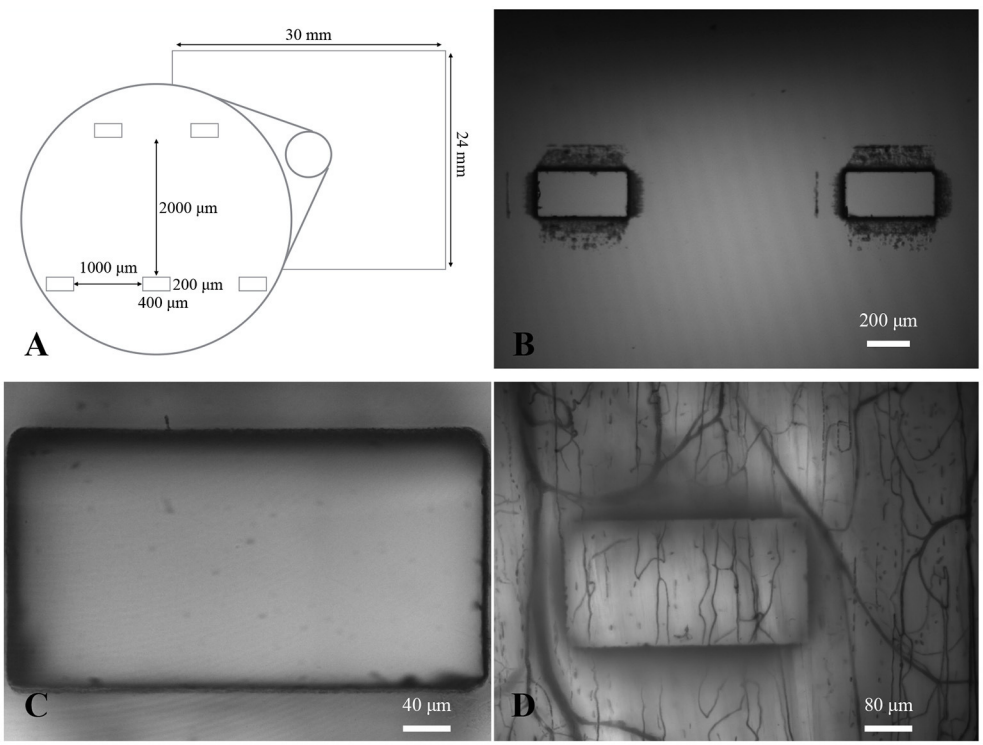

FIGURE 3 | Gas exchange window design. **(A)** Diagram of the design of the gas exchange windows. **(B)** A 4X micrograph showing two of the exchange windows centered in the field of view. Dark markings from laser machining can be seen around the edges of each window. **(C)** A 20X micrograph of an exchange window focused on the edge closest to the objective. **(D)** A 10X functional image of the minimum intensity values over time with dark lines showing location of flowing capillaries and larger micro vessels (as well as outline of the window).

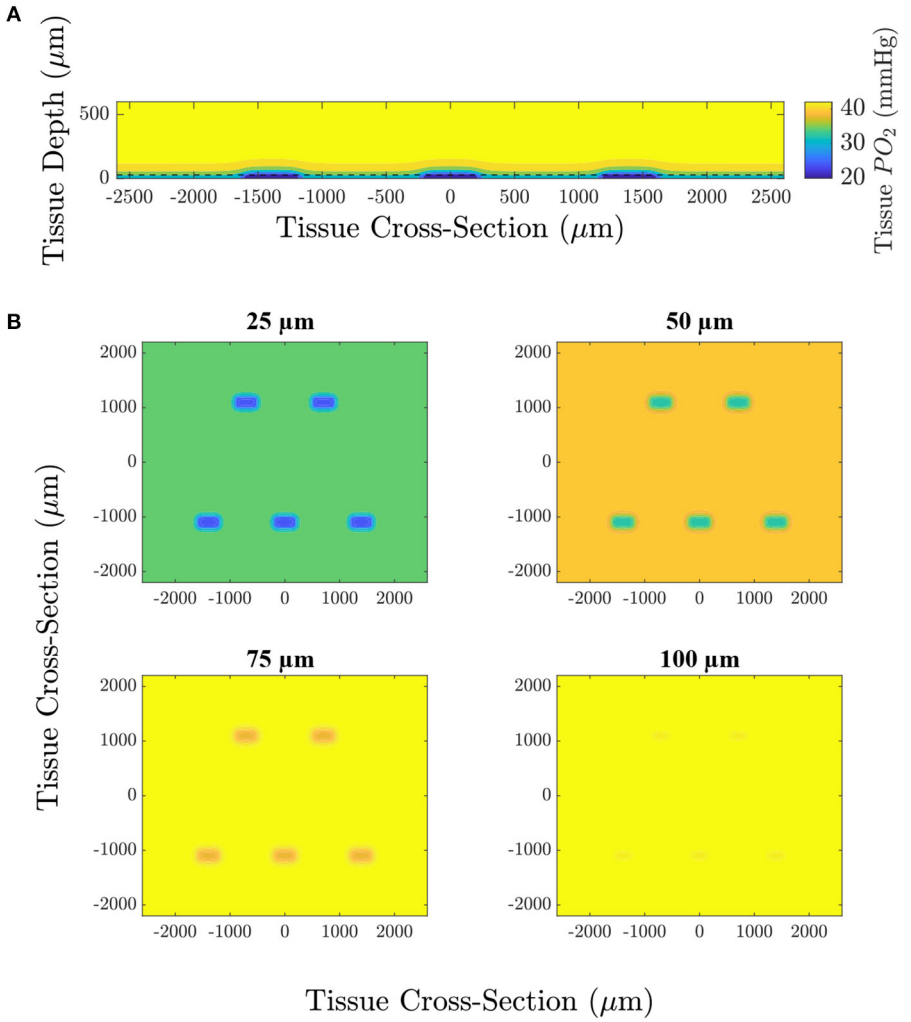

FIGURE 4 | Computational simulation predicting the tissue PO_2 resulting from diffusional exchange between the tissue and gas exchange chamber in response to a low O_2 challenge. Results are presented as a contour map of the steady-state O_2 distribution in the tissue around the gas exchange windows with a 25 µm thick PDMS layer. **(A)** Section through the long axis of the window oriented normal to the imaging plane of the microscope. The dashed line indicates the position of the top of the PDMS layer. **(B)** Sections oriented with the imaging plane at depths of 25, 50, 75, and 100 µm from the surface of the glass slide.

The temporal derivative was discretized using an implicit-explicit method similar to Ascher et al. (1995) and the spatial derivatives were discretized using a second order central difference scheme. In this scheme, the linear source term was evaluated at the current time step, where as the other terms were evaluated at the previous time step. This scheme was chosen since it is fully explicit and has greater stability than the forward Euler scheme. The numerical solution was parallelized on a GPU and implemented in C++/CUDA. The numerical grid was spatially decomposed onto a 1024-core GPU.

We quantified the extent of the O_2 perturbation in each dimension by calculating distance from the edge window in which the directional derivative of the PO_2 is less than e^{-4} ($\approx$0.02) mmHg/µm.

3. RESULTS

Five gas exchange windows were patterned into glass slides to facilitate positioning of the muscle relative to the exchange window (**Figure 3**). Windows were designed to be 200 by 400 µm. The spacing of the windows was chosen to allow for regions between the windows that are unaffected by the change in O_2. This aim was supported by the results of our mathematical model; see **Figure 4**. Dark markings from the laser cutting process can been seen around the edges of the windows; this is due to the laser fabrication process increasing light scatter near the cut edges. It can be noted that these marks only appear on one side of the glass slide. We chose the non-marked side to be in contact with the muscle to ensure that the markings are out of the

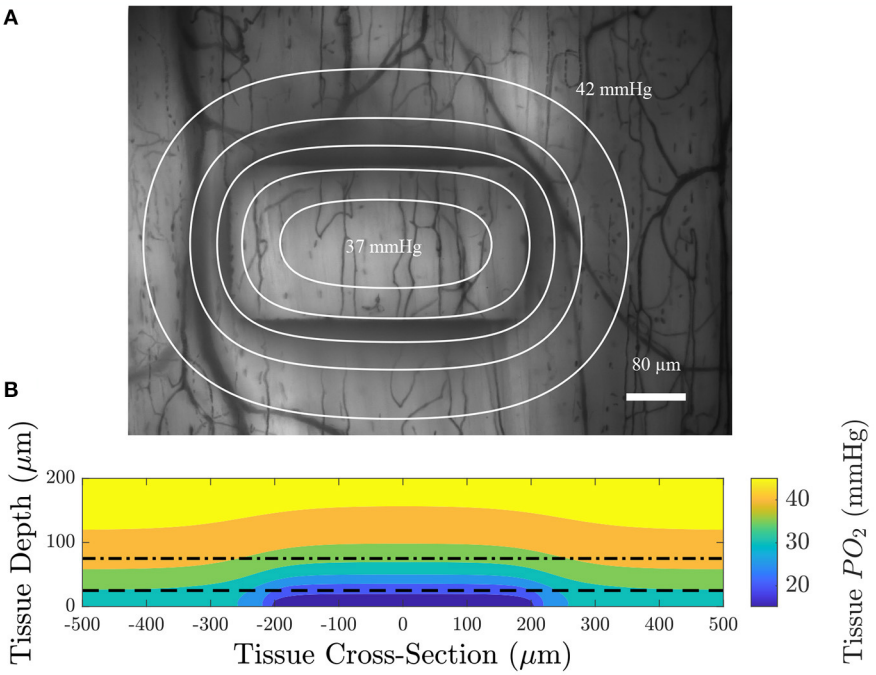

FIGURE 5 | (A) An intravital video microscopy functional image of the minimum pixel intensity over time with contour lines displaying constant PO_2 at a depth of 75 μm from the top surface of the glass slide (dotted dashed line in **B**); each contour is spaced 1 mmHg apart. **(B)** A colormap of the oxygen distribution as a function of depth in the tissue for a section through the long axis of the window; the dashed line indicates the location of the top of the PDMS layer and the dotted dashed line indicates the position of the imaging plane. The model predicts that the area affected by low oxygen challenges imposed by the gas exchange platform extend over an approximate area of 614 by 434 μm.

focal plane when focused on the muscle; this can be seen in **Figures 3C,D**.

We used a model of O_2 transport that was modified from that used in Goldman (2008) and Ghonaim et al. (2011) to predict the distribution of O_2 in the tissue and to determine the extent to which the perturbation penetrates the tissue. It should be noted that this model only considers diffusion, neglecting convective effects caused by RBCs transporting O_2 which would further limit the extent of the perturbation into the tissue. **Figure 4** shows the steady-state PO_2 distribution for a low (2%) O_2 challenge in five different planes for a large section of tissue. PO_2 distribution in a plane normal to the imaging plane of the microscope is given to show the depth of penetration of the perturbation. The largest predicted depth of penetration occurs in the center of the window, reaching a depth of 130 μm from the tissue surface. Additionally, the radial extend of the decrease in oxygen is shown by the PO_2 distribution at the tissue surface and at depths of 25, 50, and 75 μm from the exchange window surface. The decrease in tissue oxygen is predicted to extend a maximum of 109 μm from the the edge of the window in the direction of the long axis of the window and 117 μm in the direction of the short axis of the window. Due to the high solubility of O_2 in PDMS, tissue depths below ∼50 μm from the glass slide (75 μm from the surface of the glass slide) are predicted to experience non-local changes in O_2. This effect would be exacerbated for thicker PDMS layers. **Figure 5** shows the model predictions of PO_2 close to the window, with the first panel displaying contour lines over a functional microscopy image displaying the anatomical structure of the vasculature in the tissue. At this depth, the low O_2 condition is predicted to only impose SO_2 changes in capillaries directly overlying the exchange window.

To verify that the exchange window is affecting RBC SO_2, we performed step changes in chamber [O_2] and measured the resulting RBC SO_2. At baseline, the gas composition contained 5% O_2, 5% CO_2, and balance N_2. After 1 min, the gas composition was changed to 2% O_2, 5% CO_2, and balance N_2. An example of a step change for multiple capillaries in a single field of view is shown in **Figure 6**. After the drop in gas chamber O_2, the SO_2 drops rapidly then steadily increases. This increase can be explained by the increased RBC flow rate in response to the low O_2. It can also be noted that the trend is similar for all capillaries in the field of view overlying the micro-outlet.

A further demonstration of the desaturation capabilities of this device are shown in **Figure 7**. This figure shows the distribution of capillary SO_2 values when the window O_2 is set to 2, 5, and 12% (5% CO_2 and balance N_2). These results demonstrate the large variations in RBC SO_2 experienced in the microcirculation, even when subjected to variations in window O_2. The variations are due to the variability in RBC supply rate between vessels, which vary from approximately 2 RBC/s to 40 RBC/s in this example field of view.

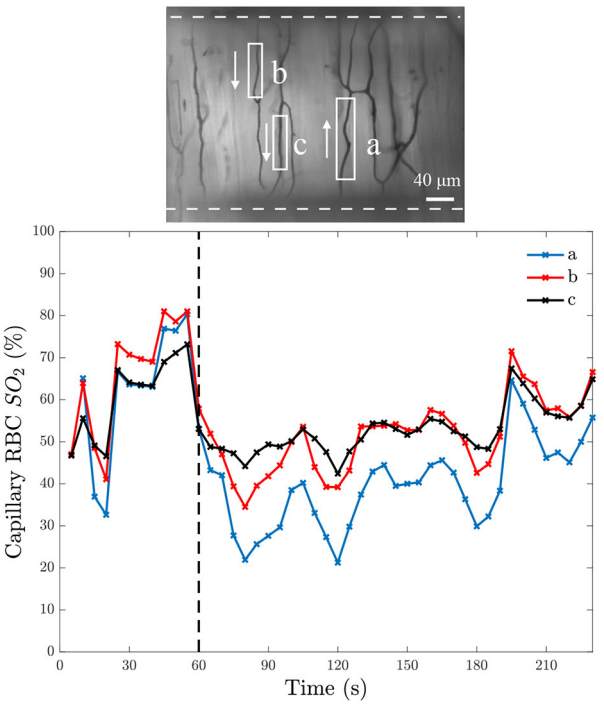

FIGURE 6 | Capillary red blood cell oxygen saturation in response to a step change in O_2. The bottom panel shows mean capillary red blood cell (RBC) oxygen saturation (SO_2) of 5-s bins from three separate capillaries in the same field of view over time; the time at which O_2 was changed is indicated with the black dashed line. The field of view from which the measurements were taken is represented by the intravital microscopy functional image of the minimum pixel intensity over the duration of the video shown in the top panel. The analyzed capillaries in the top panel are identified by white boxes, with arrows to indicate the direction of RBC flow, and the white dashed line indicates the position of the O_2 exchange window.

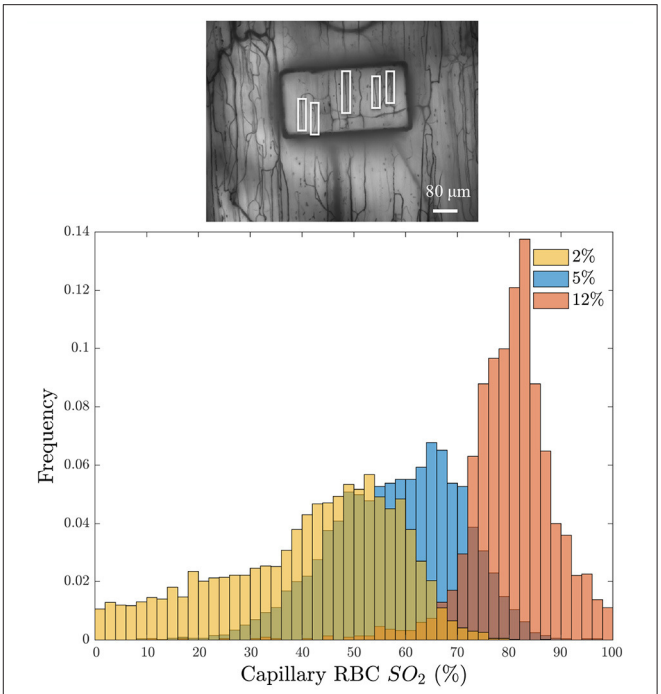

FIGURE 7 | (Bottom) Distribution of the average capillary red blood cell oxygen saturation (Capillary RBC SO_2) binned into 5-s intervals in response to three window O_2 levels: 2% (orange), 5% (blue), and 12% (red). Histogram bins are partially transparent to show the overlap. The minimum intensity functional image of the analyzed field of view is given above the histogram **(Top)**; the analyzed capillaries are indicated with white boxes.

The computational model was also used to verify how quickly changes in chamber O_2 affect tissue O_2 at varying depths in the tissue. The model assumes the gas composition at the window changes instantly; thus the model is determining the temporal diffusion limitation. **Figure 8A** shows the simulation results for a step change in O_2 from 5 to 2% centered in the window at varying tissue depths. The results of a square wave in O_2 are shown in **Figure 8B**. The simulation demonstrates that diffusion reaches steady-state within 3 s of the the step change.

To demonstrate that the device can induce flow rate responses, we measured both RBC SO_2 in selected in-focus capillaries as well as RBC supply rate in response to a square wave change in chamber [O_2]. The square wave consisted of 1 min of 5% O_2 followed by 2 min of 12%, 2 min of 2%, and 1 min of 5% with static 5% CO_2 and balance N_2. Representative responses from a single field of view from a the square wave change in platform [O_2] is shown in **Figure 9**. Responses from square-wave oscillations of capillaries directly overlying the exchange window were determined based on measurements in the last 30s of each step from 14 fields of view across 4 animals and are shown in **Figure 10**. Capillary RBC SO_2 data was not found to significantly deviate from assumed normal distributions and therefore parametric tests were applied. RBC SO_2 of capillaries directly overlying the window at the initial 5% chamber [O_2] was 60.4 ± 12.7% and was found to be significantly different than capillary RBC SO_2 at chamber concentrations of 12%, 81.3 ± 9.60%, and 2%, 50.5 ± 16.16% ($p < 0.0001$ and 0.0293 respectively, $n = 24$ capillaries). Data sets for capillary velocity, hematocrit, and supply rate were all found to deviate significantly from the assumed normal distribution and non-parametric tests were applied accordingly. The imposed chamber [O_2] caused significant changes in capillary hematocrit from the initial 5% chamber [O_2], 11.1 ± 4.59%, compared to chamber [O_2] of 12%, 7.0 ± 5.87% ($p = 0.0060$), and 2% chamber [O_2], 15.6 ± 8.63% ($p = 0.0020$, $n = 32$ capillaries). Similarly, changes in chamber [O_2] caused flow changes as measured by capillary RBC SR between the initial 5% condition, 7.9 ± 6.43, vs. 12%, 4.4 ± 5.4 cells/s ($p = 0.0020$), as well as at the 2% [O_2], 11.5 ± 10.69 ($p = 0.0060$, $n = 32$ capillaries).

The capability of the oxygen exchange platform to alter RBC SO_2 in capillaries at a distance from the exchange window was assessed for all in focus vessels < 100 µm from the window, 100–200 µm from the window, and in vessels > 200 µm from the window (**Figure 11**). Capillary RBC SO_2 data for each grouping of vessels outside of the window was not found to significantly deviate from assumed normal distributions. For vessels < 100

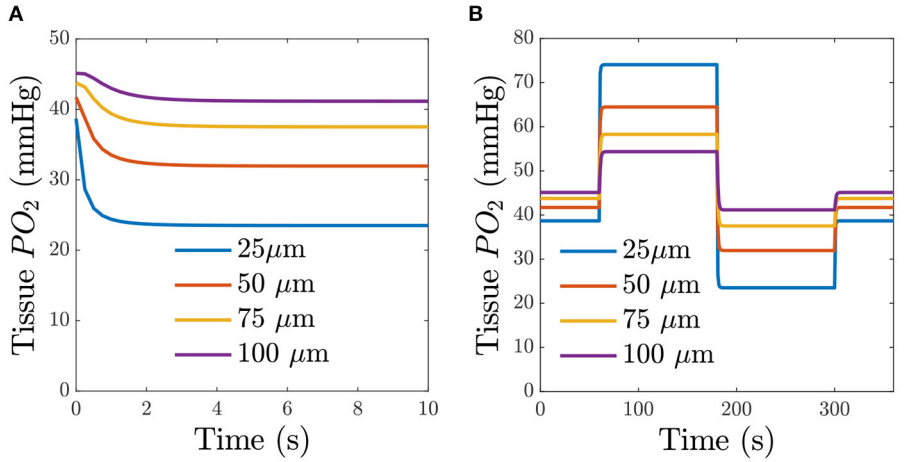

FIGURE 8 | Predicted time-dependent changes in tissue O_2. **(A)** Predicted tissue PO_2 for a step change in chamber O_2 for different depths from the glass slide. **(B)** Predicted tissue PO_2 in response to a square wave in chamber O_2. The square-wave consisted of 1 min of 5% O_2, 2 min of 12% O_2, 2 min of 2% O_2, and 1 min of 5% O_2. The legend indicates the depth from the surface of the exchange window.

μm outside the window, oscillations in chamber [O_2] caused significant changes in capillary SO_2 at 12% [O_2], 74.5 $\pm$ 10.91% (p = 0.0014), and 2% [O_2], 53.9 $\pm$ 10.84% (p = 0.0217), compared to the mean capillary SO_2 of 60.4 $\pm$ 14.17% at the initial 5% condition (n = 17 capillaries). Similarly, significant changes in SO_2 were found in capillaries 100–200 μm from the window at 12% [O_2], 73.9 $\pm$ 12.24% (p < 0.0001), and 2% [O_2], 59.5 $\pm$ 11.68% (p = 0.0252), compared to the capillary SO_2 of 64.0 $\pm$ 13.32% at the initial 5% condition (n = 27 capillaries). In vessels > 200 μm from the window no significant change in capillary SO_2 compared to the initial 5% [O_2] was detected (63.6 $\pm$ 12.48%), although SO_2 was significantly different between the 12 and 2% conditions, 68.6 $\pm$ 14.22% and 57.8 $\pm$ 16.23% (p = 0.0005, n = 20 capillaries). No robust changes in mean capillary hemodynamic measures were noted for vessels at a distance from the window grouped by the three distance delineations described above (data not shown).

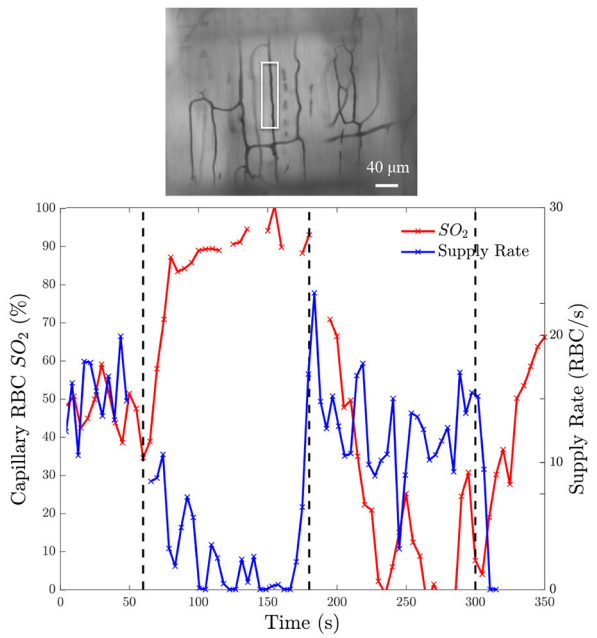

FIGURE 9 | Oxygen saturation and supply rate change in response to square wave oxygen challenge from a baseline of 5% O_2 followed by 2 min of 12%, 2 min of 2%, and 1 min of 5% with 5% CO_2 and balance N_2. **(Bottom)** Induced SO_2 changes is given on the left ordinate axis and the corresponding change in RBC supply rate is given on the right ordinate axis. The black dashed lines indicate the time at which the chamber O_2 was changed. The analyzed capillary is indicated with a white box in the minimum intensity functional image above the figure **(Top)**.

4. DISCUSSION

In this study, we developed a modular gas exchange platform to deliver a localized gas composition to the surface of externalized EDL muscle tissue for use in intravital microscopy studies. Our model predicts that the platform is able to change RBC SO_2 in capillaries within a localized area of approximately 614 by 434 μm (**Figure 5**). The changes in capillary RBC SO_2 were demonstrated both experimentally (**Figures 6**, **7**, **10**, **11**) and computationally (**Figure 5**); the later predicts that the effect of the perturbation extends to a maximum of 117 μm beyond the edge of the window which is an important and novel insight resulting from the present work. This diffusive spread of PO_2 within the exchange membrane has not previously been reported as earlier studies did not include the exchange membrane itself as an element of the model (Ghonaim et al., 2011, 2013). Additionally, our experimental results demonstrate that the changes in tissue PO_2 propagate even further than our mathematical model predicts with measurable changes in capillary SO_2 extending

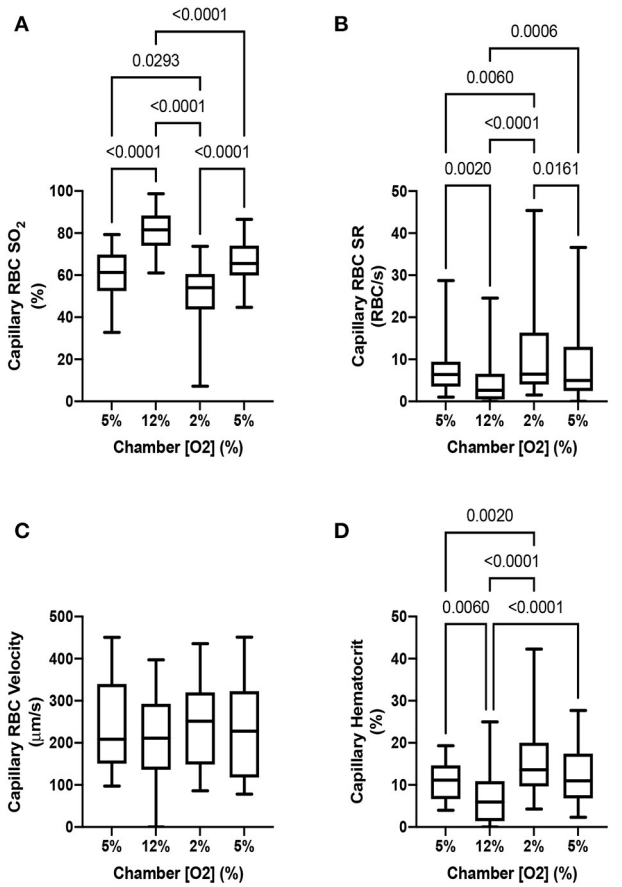

FIGURE 10 | Capillary hemodynamics and oxygen saturation responses in capillaries directly overlying exchange windows of the modular gas exchange platform. The platform imposed a square wave oxygen challenge from a baseline of 5% O_2 chamber oxygen concentration ([O_2]) followed by 2 min of 12%, 2 min of 2%, and 1 min of 5% with 5% CO_2 and balance N_2. **(A)** shows the capillary red blood cell (RBC) oxygen saturation (SO_2) in the last 30s of each imposed chamber [O_2] across 14 fields in 4 animals (n = 24 capillaries). The resulting blood flow response to the change in SO_2 is illustrated by the capillary RBC supply rate (SR) and hematocrit changes shown in **(B,D)** (n = 32 capillaries). Changes in capillary RBC velocity **(C)** were not found to be significant between any chamber [O_2] (n = 29 capillaries). p values based on Tukey's multiple comparisons test after significant repeated measures ANOVA (capillary RBC SO_2), and Dunn's multiple comparisons test after significant Friedman test (capillary RBC SR and hematocrit) are indicated in the figure with a $p < 0.05$ considered to be significant. Box and whisker plots show minimum, median, maximum, and associated quartiles.

beyond 200 μm (**Figure 11**). The discordance between our model's prediction and the experimental result is likely due to a mismatch in assumed model parameters, particularly muscle oxygen consumption; our present model also does not consider the specific microvascular geometry and spatial location of vessels within the volume which is likely to contribute to the difference between the predicted change in tissue PO_2 and the observed SO_2 changes. This is an important consideration for future studies seeking to spatially constrain oxygen challenges to specific vascular structures or regions of interest. The computational model also predicts that O_2 diffusion into the tissue will reach steady-state within 3 s of changing the chamber O_2. As with the distance to which the low oxygen challenge extends into the tissue, the prediction for this time transient may be impacted by the location of individual blood vessels within the tissue, for which the model does not account.

In previous work, we used a smaller gas exchange window to induce capillary RBC SO_2 changes (Ghonaim et al., 2011). Ghonaim et al. suggested that not enough capillaries were stimulated to elicit a flow response (Ghonaim, 2013; Ghonaim et al., 2013). This is supported by the use of a larger gas exchange window to induce RBC SO_2 changes in more capillaries to which the vasculature responded (Ghonaim, 2013). In the current study, we used a window size (400 × 200 μm rectangular window) that was larger than that used in Ghonaim et al. (2011) (100 μm diameter circular window) but smaller than that used in Ghonaim (2013) (1.000 × 200 μm rectangular window). Our present configuration was capable of imposing significant changes in capillary SO_2 and concomitant hemodynamic responses in vessels directly overlying the exchange window (**Figure 10**). The changes in SO_2 in both (Ghonaim et al., 2011; Ghonaim, 2013) were consistent with those in our chamber. This finding supports the hypothesis that the ATP release signal is additive since we are affecting more capillaries than in Ghonaim et al. (2011).

Various studies in the literature have been successful in imposing changes in RBC SO_2 both *in vivo* and *ex vivo* (Duling, 1972; Pittman and Duling, 1973; Hutchins et al., 1974; Fredricks et al., 1994; Welsh et al., 1998; Zhu et al., 1998; Frisbee and Lombard, 2002; Frisbee et al., 2002). One approach is to alter the inspired O_2 levels as in Zhu et al. (1998), resulting in changed RBC SO_2, though this may result in systemic hyper/hypoxia (Jackson, 2016). Another approach involves using superfusion solutions with different gas compositions to bathe the tissue in order to control the surface O_2 levels (Frisbee and Lombard, 2002; Frisbee et al., 2002). While this method confines the changes in O_2 to the tissue being studied, due to the low solubility of O_2 in water, superfusion solutions have a limited ability to change SO_2 and lacks spatial specificity, particularly as it pertains to the levels of vasculature being affected. Additionally, our current approach is able to produce a more rapid change in PO_2 compared to those using superfusion solutions. For these reasons, gas exchange chambers may be more advantageous compared to other approaches in the investigations of localized O_2 regulation.

Despite the many benefits of the approach employed in this work, there are a few challenges that are worth noting. Firstly, due to the micro-outlet patterned in the glass, the tissue viewed through the window opening is in a different focal plane than the surrounding tissue at the same depth of focus. Because of this, it is not possible to focus on capillaries in and out of the window at the same tissue depth simultaneously. However, due to the excellent optical clarity outside the window, it is possible to focus on capillaries outside of the window, enabling measurement of unperturbed hemodynamics and SO_2 levels in the tissue at a sufficient distance from the window.

Another challenge associated with this experiment is placement of the muscle over the exchange windows. This

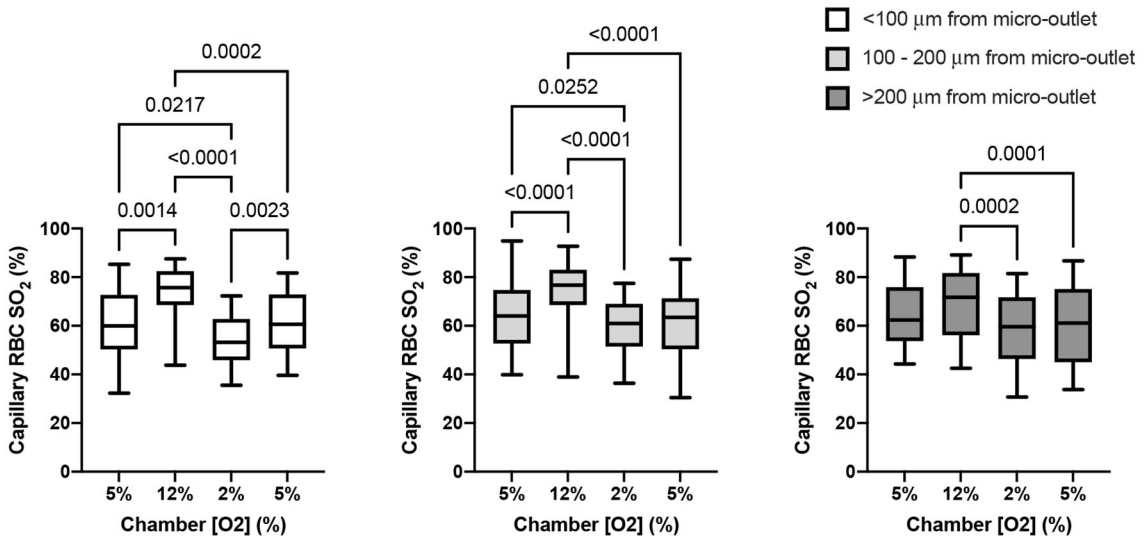

FIGURE 11 | Capillary oxygen saturation responses in capillaries at various distances from the exchange windows of the modular gas exchange platform. The platform imposed a square wave oxygen challenge from a baseline of 5% O_2 followed by 2 min of 12%, 2 min of 2%, and 1 min of 5% each with 5% CO_2 and balance N_2. Each panel shows the capillary red blood cell (RBC) oxygen saturation (SO_2) in the last 30s of each imposed platform oxygen concentration across 14 fields in 4 animals. The left panel shows oxygen saturations in capillaries within < 100 μm from the exchange window ($n = 17$ capillaries). The middle panel shows mean capillary RBC SO_2 in vessels between 100 and 200 μm from the window ($n = 27$ capillaries), and the right panel shows responses in capillaries > 200 μm from the edge of the exchange window ($n = 19$ capillaries). With increasing distance the magnitude of the SO_2 change diminishes, though significant changes in SO_2 imposed by the low oxygen condition in the platform were detectable beyond 200 μm. p values based on Tukey's multiple comparisons test after significant repeated measures ANOVA are indicated in the figure with a $p < 0.05$ considered to be significant. Box and whisker plots show minimum, median, maximum, and associated quartiles.

requires careful manipulation of the muscle in order to place the muscle over the windows such that the imposed perturbation would affect capillary modules of interest. This is an important consideration since moving the muscle multiple times may increase the likelihood of the muscle becoming stressed and impairing the vasculature to respond to changes in O_2. Including additional windows closer together would increase the probability of one of the windows being over an area of interest in the muscle, though care must be taken to ensure that the other windows do not interact with vessels in the region being observed.

Our device is well-suited to studying oxygen regulation at the microvascular level. For example, our method could be used to interrogate whether changes in capillary RBC distribution are due to passive rheology (i.e., bifurcation law) or if there are other active mechanisms in place, such as pericytes that respond to changes in O_2 to control flow in capillaries. Indeed, Ellis et al. (1994) showed that as supply rate increases, the distribution of flow becomes more homogenous. To determine if this effect is purely due to passive rheology, one could position the window over capillaries fed from the same arteriole to identify if their distribution of flow rates among the capillaries remains constant in response to oxygen. Further, this platform could be used to determine if stimulating capillaries in one capillary module affects adjacent modules connected to the same feed arteriole. Such an experiment could help support the SO_2-dependent ATP release from RBC hypothesis. Conversely, if the O_2 sensor is located in the extravascular space rather than the RBCs, the O_2 exchange platform could further be used to stimulate areas of the muscle that lack capillaries to investigate the presence of a tissue sensor.

Additionally, this approach could be used in *ex vivo* and *in vitro* studies where the control of gas composition needs to be locally confined. For example, this gas exchange platform could be used in conjunction with a microfluidic device to desaturate flowing RBCs as suggested in Sove et al. (2013) and Sové et al. (2016). As proposed in these studies, such a device could probe the dynamics of the ATP release mechanism if it is indeed caused by RBC desaturation.

In summary, we have developed a modular gas exchange platform capable of causing local changes in capillary RBC SO_2 and stimulating corresponding responses in capillary hemodynamics. We have also shown that these changes are consistent with the ATP release hypothesis that multiple capillaries need to be stimulated in order to elicit a microvascular flow rate response. While our device stimulates a large enough region to obtain a flow response, it is also localized enough that we will be able to probe specific spatial regions in the microvascular bed, and the device's excellent optical clarity allows for direct observation of the response both in the stimulated, as well as neighboring regions. This tool offers exciting possibilities to study microvascular oxygen regulation, and may aid to definitively determine the location of the elusive oxygen sensor.

DATA AVAILABILITY STATEMENT

The data supporting the conclusions of this article will be made available by the authors, without undue reservation.

ETHICS STATEMENT

The animal study was reviewed and approved by University of Western Ontario's Animal Care and Use Committee.

AUTHOR CONTRIBUTIONS

This study was conceived and designed by RS, CE, and GF. The modular gas exchange chamber was designed by RS, DH, and HN aided in the fabrication. RS and SM collected the *in vivo* experimental data. RS wrote the mathematical model and generated the resulting simulation data. Data analysis and interpretation was done by RS, SM, CE, and GF. RS wrote the manuscript with input from all authors. Critical revision was done by RS, CE, and GF.

FUNDING

This work was supported by the Natural Sciences and Engineering Research Council of Canada Discovery grants RGPIN 2017-05205 (GF), R1379A13 (CE), and RGPIN-2019-07209 (CE). NSERC funding supplied resources for experimental materials, equipment, technical support, and trainee stipends. RS was supported by a Natural Sciences and Engineering Research Council of Canada Graduate Scholarship.

REFERENCES

Arpino, J. M., Nong, Z., Li, F., Yin, H., Ghonaim, N., Milkovich, S., et al. (2017). Four-dimensional microvascular analysis reveals that regenerative angiogenesis in ischemic muscle produces a flawed microcirculation. *Circ. Res.* 120, 1453–1465. doi: 10.1161/CIRCRESAHA.116.310535

Ascher, U. M., Ruuth, S. J., and Wetton, B. T. (1995). Implicit-explicit methods for time-dependent partial differential equations. *SIAM J. Numer. Anal.* 32, 797–823. doi: 10.1137/0732037

Bateman, R. M., Sharpe, M. D., Jagger, J. E., and Ellis, C. G. (2015). Sepsis impairs microvascular autoregulation and delays capillary response within hypoxic capillaries. *Crit. Care* 19:389. doi: 10.1186/s13054-015-1102-7

Bentley, T. B., Meng, H., and Pittman, R. N. (1993). Temperature dependence of oxygen diffusion and consumption in mammalian striated muscle. *Am. J. Physiol. Heart Circ. Physiol.* 264, H1825–H1830. doi: 10.1152/ajpheart.1993.264.6.H1825

Bergfeld, G., and Forrester, T. (1992). Release of ATP from human erythrocytes in response to a brief period of hypoxia and hypercapnia. *Cardiovasc. Res.* 26, 40–47. doi: 10.1093/cvr/26.1.40

Collins, D. M., McCullough, W. T., and Ellsworth, M. L. (1998). Conducted vascular responses: communication across the capillary bed. *Microvasc. Res.* 56, 43–53. doi: 10.1006/mvre.1998.2076

Dietrich, H. H., Ellsworth, M. L., Sprague, R. S., and Dacey Jr, R. G. (2000). Red blood cell regulation of microvascular tone through adenosine triphosphate. *Am. J. Physiol. Heart Circ. Physiol.* 278, H1294–H1298. doi: 10.1152/ajpheart.2000.278.4.H1294

Duling, B. R. (1972). Microvascular responses to alterations in oxygen tension. *Circ. Res.* 31, 481–489. doi: 10.1161/01.RES.31.4.481

Ellis, C., Milkovich, S., and Goldman, D. (2006). Experimental protocol investigating local regulation of oxygen supply in rat skeletal muscle *in vivo*. *J. Vasc. Res.* 43:45. doi: 10.1159/000094939

Ellis, C., Wrigley, S., and Groom, A. (1994). Heterogeneity of red blood cell perfusion in capillary networks supplied by a single arteriole in resting skeletal muscle. *Circ. Res.* 75, 357–368. doi: 10.1161/01.RES.75.2.357

Ellis, C. G., Ellsworth, M. L., Pittman, R. N., and Burgess, W. L. (1992). Application of image analysis for evaluation of red blood cell dynamics in capillaries. *Microvasc. Res.* 44, 214–225.

Ellis, C. G., Goldman, D., Hanson, M., Stephenson, A. H., Milkovich, S., Benlamri, A., et al. (2010). Defects in oxygen supply to skeletal muscle of prediabetic ZDF rats. *Am. J. Physiol. Heart Circ. Physiol.* 298, H1661–H1670. doi: 10.1152/ajpheart.01239.2009

Ellsworth, M. L., Ellis, C. G., Goldman, D., Stephenson, A. H., Dietrich, H. H., and Sprague, R. S. (2009). Erythrocytes: oxygen sensors and modulators of vascular tone. *Physiology* 24, 107–116. doi: 10.1152/physiol.00038.2008

Ellsworth, M. L., Forrester, T., Ellis, C. G., and Dietrich, H. H. (1995). The erythrocyte as a regulator of vascular tone. *Am. J. Physiol. Heart Circ. Physiol.* 269, H2155–H2161.

Fraser, G. M., Milkovich, S., Goldman, D., and Ellis, C. G. (2012). Mapping 3-D functional capillary geometry in rat skeletal muscle *in vivo*. *Am. J. Physiol. Heart Circ. Physiol.* 302, H654–H664. doi: 10.1152/ajpheart.01185.2010

Fredricks, K., Liu, Y., and Lombard, J. H. (1994). Response of extraparenchymal resistance arteries of rat skeletal muscle to reduced PO_2. *Am. J. Physiol. Heart Circ. Physiol.* 267, H706–H715. doi: 10.1152/ajpheart.1994.267.2.H706

Frisbee, J. C., and Lombard, J. H. (2002). Parenchymal tissue cytochrome P450 4A enzymes contribute to oxygen-induced alterations in skeletal muscle arteriolar tone. *Microvasc. Res.* 63, 340–343. doi: 10.1006/mvre.2002.2409

Frisbee, J. C., Maier, K. G., Falck, J. R., Roman, R. J., and Lombard, J. H. (2002). Integration of hypoxic dilation signaling pathways for skeletal muscle resistance arteries. *Am. J. Physiol. Regul. Integr. Compar. Physiol.* 283, R309–R319. doi: 10.1152/ajpregu.00741.2001

Ghonaim, N. W. (2013). Investigating Conducted Microvascular Response To Localized Oxygen Delivery In Vivo Using A Novel Micro-Delivery Approach. PhD Thesis, University of Western Ontario. Electronic Thesis and Dissertation Repository. 1643. Available online at: https://ir.lib.uwo.ca/etd/1643

Ghonaim, N. W., Fraser, G. M., Ellis, C. G., Yang, J., and Goldman, D. (2013). Modeling steady state SO_2-dependent changes in capillary ATP concentration using novel O_2 micro-delivery methods. *Front. Physiol.* 4:260. doi: 10.3389/fphys.2013.00260

Ghonaim, N. W., Lau, L. W., Goldman, D., Ellis, C. G., and Yang, J. (2011). A micro-delivery approach for studying microvascular responses to localized oxygen delivery. *Microcirculation* 18, 646–654. doi: 10.1111/j.1549-8719.2011.00132.x

Goldman, D. (2008). A mathematical model of oxygen transport in intact muscle with imposed surface oscillations. *Math. Biosci.* 213, 18–28. doi: 10.1016/j.mbs.2008.01.010

Golub, A. S., and Pittman, R. N. (2013). Bang-bang model for regulation of local blood flow. *Microcirculation* 20, 455–483. doi: 10.1111/micc.12051

Hanson, M. S., Ellsworth, M. L., Achilleus, D., Stephenson, A. H., Bowles, E. A., Sridharan, M., et al. (2009). Insulin inhibits low oxygen-induced atp release from human erythrocytes: implication for vascular control. *Microcirculation* 16, 424–433. doi: 10.1080/10739680902855218

Honig, C., and Gayeski, T. (1982). Correlation of O_2 transport on the micro and macro scale. *Int. J. Microcirc. Clin. Exp.* 1, 367–380.

Hutchins, P. M., Bond, R. F., and Green, H. D. (1974). Participation of oxygen in the local control of skeletal muscle microvasculature. *Circ. Res.* 34, 85–93.

Jackson, W. F. (2016). Arteriolar oxygen reactivity: where is the sensor and what is the mechanism of action? *J. Physiol.* 594, 5055–5077. doi: 10.1113/JP270192

Jagger, J., McCullen, S., Yun, C., and Ellis, C. (2004). Erythrocyte hemodynamics as a function of the local o2 environment in the edl muscle of the rat. *FASEB J.* 18:A632.

Japee, S. A., Ellis, C. G., and Pittman, R. N. (2004). Flow visualization tools for image analysis of capillary networks. *Microcirculation* 11, 39–54. doi: 10.1080/10739680490266171

Japee, S. A., Pittman, R. N., and Ellis, C. G. (2005a). Automated method for tracking individual red blood cells within capillaries to

compute velocity and oxygen saturation. *Microcirculation* 12, 507–515. doi: 10.1080/10739680591003341

Japee, S. A., Pittman, R. N., and Ellis, C. G. (2005b). A new video image analysis system to study red blood cell dynamics and oxygenation in capillary networks. *Microcirculation* 12, 489–506. doi: 10.1080/10739680591003332

Kontos, H. A., and Wei, E. P. (1985). Oxygen-dependent mechanisms in cerebral autoregulation. *Ann. Biomed. Eng.* 13, 329–334. doi: 10.1007/BF02584251

Mahler, M., Louy, C., Homsher, E., and Peskoff, A. (1985). Reappraisal of diffusion, solubility, and consumption of oxygen in frog skeletal muscle, with applications to muscle energy balance. *J. Gen. Physiol.* 86, 105–134.

McCullough, W. T., Collins, D. M., and Ellsworth, M. L. (1997). Arteriolar responses to extracellular ATP in striated muscle. *Am. J. Physiol. Regul. Integr. Compar. Physiol.* 272, H1886–H1891.

McDonald, J. C., Duffy, D. C., Anderson, J. R., Chiu, D. T., and Wu, H. (2000). Fabrication of microfluidic systems in poly(dimethylsiloxane). *Electrophoresis* 21, 27–40. doi: 10.1002/(SICI)1522-2683(20000101)21:1<27::AID-ELPS27>3.0.CO;2-C

Merkel, T., Bondar, V., Nagai, K., Freeman, B., and Pinnau, I. (2000). Gas sorption, diffusion, and permeation in poly (dimethylsiloxane). *J. Polym. Sci. Part B Polym. Phys.* 38, 415–434. doi: 10.1002/(SICI)1099-0488(20000201)38:3<415::AID-POLB8>3.0.CO;2-Z

Milkovich, S. L., MacKie, M., Goldman, D., and Ellis, C. G. (2007). Local regulation of oxygen supply in rat skeletal muscle *in vivo*: variations in hemodynamic response. *FASEB J.* 21:A481. doi: 10.1096/fasebj.21.5.A481-d

Nikumb, S., Chen, Q., Li, C., Reshef, H., Zheng, H., Qiu, H., et al. (2005). Precision glass machining, drilling and profile cutting by short pulse lasers. *Thin Solid Films* 477, 216–221. doi: 10.1016/j.tsf.2004.08.136

Pittman, R. N., and Duling, B. R. (1973). Oxygen sensitivity of vascular smooth muscle: I. *In vitro* studies. *Microvasc. Res.* 6, 202–211.

Shiku, H., Saito, T., Wu, C.-C., Yasukawa, T., Yokoo, M., Abe, H., et al. (2006). Oxygen permeability of surface-modified poly (dimethylsiloxane) characterized by scanning electrochemical microscopy. *Chem. Lett.* 35, 234–235. doi: 10.1246/cl.2006.234

Sové, R. J., Fraser, G. M., Goldman, D., and Ellis, C. G. (2016). Finite element model of oxygen transport for the design of geometrically complex microfluidic devices used in biological studies. *PLOS ONE* 11:e0166289. doi: 10.1371/journal.pone.0166289

Sove, R. J., Ghonaim, N., Goldman, D., and Ellis, C. G. (2013). A computational model of a microfluidic device to measure the dynamics of oxygen-dependent ATP release from erythrocytes. *PLoS ONE* 8:e81537. doi: 10.1371/journal.pone.0081537

Sparks, H. V. (1980). "Effect of local metabolic factors on vascular smooth muscle," in *Handbook of Physiology, Section 2, The Cardiovascular System, Vol. II, Vascular Smooth Muscle*, eds D. F. Bohr, A. P. Somlyo, and H. V. Sparks (Bethesda, MD: American Physiological Society), 475–513.

Sprague, R. S., Ellsworth, M. L., Stephenson, A. H., and Lonigro, A. J. (1996). ATP: the red blood cell link to no and local control of the pulmonary circulation. *Am. J. Physiol. Regul. Integr. Compar. Physiol.* 271, H2717–H2722.

Sprague, R. S., Stephenson, A. H., Bowles, E. A., Stumpf, M. S., and Lonigro, A. J. (2006). Reduced expression of Gi in erythrocytes of humans with type 2 diabetes is associated with impairment of both cAMP generation and ATP release. *Diabetes* 55, 3588–3593. doi: 10.2337/db06-0555

Sullivan, S. M., and Pittman, R. N. (1984). *In vitro* O_2 uptake and histochemical fiber type of resting hamster muscles. *J. Appl. Physiol.* 57, 246–253.

Tyml, K., and Budreau, C. (1991). A new preparation of rat extensor digitorum longus muscle for intravital investigation of the microcirculation. *Int. J. Microcirc. Clin. Exp.* 10, 335–343.

Welsh, D. G., Jackson, W. F., and Segal, S. S. (1998). Oxygen induces electromechanical coupling in arteriolar smooth muscle cells: a role for L-type Ca^{2+} channels. *Am. J. Physiol. Regul. Integr. Compar. Physiol.* 274, H2018–H2024.

Zhu, Y., Park, T., and Gidday, J. M. (1998). Mechanisms of hyperoxia-induced reductions in retinal blood flow in newborn pig. *Exp. Eye Res.* 67, 357–369. doi: 10.1006/exer.1998.0535

Conflict of Interest: The authors declare that the research was conducted in the absence of any commercial or financial relationships that could be construed as a potential conflict of interest.